Structural and functional characterization of Sticholysin III: A newly discovered actinoporin within the venom of the sea anemone *Stichodactyla helianthus*.

Esperanza Rivera-de-Torre[1,2,3], Juan Palacios-Ortega[1,2], Jessica E. Garb[3], J. Peter Slotte[2], José G. Gavilanes[1] and Álvaro Martínez-del-Pozo[1]

[1]Departamento de Bioquímica y Biología Molecular, Facultad de Ciencias Químicas, Universidad Complutense de Madrid, Madrid, Spain.
[2]Biochemistry, Faculty of Science and Engineering, Åbo Akademi University, Turku, Finland.
[3]Department of Biological Sciences, University of Massachusetts Lowell, Lowell, MA, USA.

Correspondence: Álvaro Martínez-del-Pozo (alvaromp@quim.ucm.es), Departamento de Bioquímica y Biología Molecular, Facultad de Química, Universidad Complutense, 28040 Madrid, Spain, Telephone: 34 91 3944158.

Keywords: Pore-forming-toxin, equinatoxin, fragaceatoxin, oligomerization.

Abbreviations: CD, circular dichroism; Chol, cholesterol; DOPC, dimonounsaturated (18:1) phosphatidylcholine; ITC, isothermal titration calorimetry; LUVs, large unilamelar vesicles; PFP, pore-forming-protein; SM, sphingomyelin; Stn, sticholysin.

Abstract

Actinoporins are a family of pore-forming toxins produced by sea anemones as part of their venomous cocktail. These proteins remain soluble and stably folded in aqueous solution, but when interacting with sphingomyelin-containing lipid membranes, they become integral oligomeric membrane structures that form a pore permeable to cations, which leads to cell death by osmotic shock. Actinoporins appear as multigenic families within the genome of sea anemones: several genes encoding very similar actinoporins are detected within the same species. The Caribbean Sea anemone *Stichodactyla helianthus* produces three actinoporins (sticholysins I, II and III; StnI, StnII and StnIII) that differ in their toxic potency. For example, StnII is about four-fold more effective than StnI against sheep erythrocytes in causing hemolysis, and both show synergy. However, StnIII, recently discovered in the *S. helianthus* transcriptome, has not been characterized so far. Here we describe StnIII's spectroscopic and functional properties and show its potential to interact with the other Stns. StnIII seems to maintain the well-preserved fold of all actinoporins, characterized by a high content of β-sheet, but it is significantly less thermostable. Its functional characterization shows that the critical concentration needed to form active pores is higher than for either StnI or StnII, suggesting differences in behavior when oligomerizing on membrane surfaces. Our results show that StnIII is an interesting and unexpected piece in the puzzle of how this Caribbean Sea anemone species modulates its venomous activity.

Introduction

Protein components of venoms often appear as multigene families: A single animal species usually expresses several isotoxins as products of different genes. Such isotoxins are usually highly similar but display distinct activities derived from sequence differences among them [1-6]. This is also the case of actinoporins, highly representative protein toxins from the venom of sea anemones. Actinoporins are cytolysins which belong to the α-pore-forming-proteins (α-PFPs) family [7, 8]. These toxins remain stably folded, monomeric and soluble in water solution, but upon interaction with cell membranes of specific composition, they become oligomeric transmembrane structures [9-12], forming assemblies of different stoichiometries that lead to the final pores that produce the death of the targeted cell by osmotic shock [10-12]. In particular, the pore-formation triggering condition for actinoporins is the presence of sphingomyelin (SM) within the target cell membrane. All actinoporins whose water-soluble three-dimensional structure has been solved share a common fold pattern [13-18]. It consists of a compact hydrophobic β-sandwich core flanked by two α-helices (Figure 1A). Within this structural arrangement, it is also well-known that their N-terminal α-helix plays a key role in their pore-forming activity [6, 16, 18-26], since this protein stretch detaches from the β-sandwich core and extends to become a rather long α-helix, which is responsible for penetrating the membrane and forming the pore walls [12, 24, 27-32].

It is well known that the Caribbean sea anemone *Stichodactyla helianthus* produces two easily detectable actinoporin variants: sticholysin I (StnI) and sticholysin II (StnII) [4, 33, 34]. Both have been very well characterized, and their three-dimensional structures are known with atomic resolution. They show an almost identical conformation, in good agreement with their 93% sequence identity at the amino acid level (Figure 2) [15, 17] and the aforementioned actinoporins common fold [13-18]. The StnI isotoxin is approximately four-fold less effective than StnII in terms of hemolytic activity [4, 6]. Interestingly, StnI and StnII display synergy when assayed together. Trace amounts of StnII enhance StnI binding affinity to cell membranes, driving a dramatic improvement of hemolytic activity [35]. This StnI-StnII interacting behavior seems to be the basis for expanding the complexity and regulatory capacity of these toxins' action, potentially increasing the range of species *S. helianthus* could capture or defend itself from.

Transcriptomic profiling of venomous animals has been used as an effective approach for discovering new bioactive compound. *S. helianthus*'s transcriptome was successfully assembled and through the consequent study, the venom composition was annotated [34]. This bioinformatic analysis revealed the existence of at least one more sticholysin isoform, which was designated as StnIII. Phylogenetic analysis revealed that this StnIII is more closely related to other species' actinoporins rather than to the other Stn isotoxins produced by *S. helianthus* [34], an interesting feature from the evolutionary point of view. At the protein level, StnIII is only 76% identical to StnI and 77% to StnII (Figure 2), while StnI and StnII share 93% of their protein sequence. This sequence conservation was still similar enough to allow the prediction of StnIII's three-dimensional structure, which resulted in a conformation perfectly compatible with the actinoporins' standard fold [15, 17, 34]. However, even if StnIII's three-dimensional structure resembles that of StnI and StnII, amino acid sequence comparison showed significant differences, especially at their N-terminal stretches, which might also lead to functional differences (Figure 2). This greater divergence of StnIII relative to both Stn I and II reinforces the need to functionally evaluate its role in *S. helianthus* venom, given its potential to modulate the toxicity of the other Stns known. To this end, we have produced StnIII in *Escherichia coli*, and then purified and characterized it at spectroscopic and functional levels. The results obtained reveal different characteristics when compared to previously known Stns, allowing to us to hypothesize a potential role for StnIII within the venomous arsenal of *S. helianthus*.

Materials and methods

StnIII cloning for production in E. coli

The complete cDNA sequence coding for StnIII, signal peptide included, had been previously determined and deposited in NCBI's GenBank database (MH327769) [34]. Thus, in order to amplify and clone the mature form of StnIII (without its signal peptide) (Figure 2), two deoxyoligonucleotides were designed: 5'ACA*GAATTC*ATTAAAGAGGAGAAATTAACC**ATG**AATCCTTTAGC3' and 5'ATT*AAGCTT***TTA**GTGAGAGATCTCAATTTGCAG3'. Restriction sites for EcoRI (GAATTC) and HindIII (AAGCTT) (as italic letters in the sequences), and the corresponding initial (ATG) and stop (TAA) codons (bold letters) were included in these oligonucleotides. The amplified PCR product was digested with both restriction enzymes and cloned within a modified version of the pQE60 plasmid, which constitutes the optimized approach used by our group to produce Stns in *E. coli* in milligram amounts [36, 37].

Protein production and purification

The procedure used for the production and purification of the three actinoporins used in this study (StnI, II, and III) has been previously described in detail [6, 36, 37]. Protein production in RB791 *E. coli* cells is induced at OD_{600} of 1.0 with 1 mM IPTG for 4 h at 37 °C. Then, cells are harvested, and the cellular pellet is subjected to seven pulses of sonication (20 kc, 1 min) in an ice bath. HCl-Tris buffer (50 mM) including 1 % (v/v) Tween 20 is employed; buffer pH values (6.5 for StnI, 7.5 for StnII, and 8.5 for StnIII) were set depending on the theoretical pI value of each Stn. The water-soluble fraction of this homogenate is loaded onto a carboxymethylcellulose CM52 ion-exchange chromatography column (Whatman, Brentford, England, UK), and eluted with a NaCl gradient (0-0.3 M NaCl StnI, 0-0.5 M NaCl for StnII or 0-0.6M NaCl for StnIII) in 50 mM HCl-Tris buffer, after appropriate washing steps.

Homogeneity of protein preparations and structural spectroscopic characterization

All protein samples were purified to homogeneity in mg amounts according to their electrophoretic behavior analyzed by 0.1 % (w/v) SDS−15 % (w/v) PAGE [38]. Western blots were performed according to standardized procedures described before [35, 39], using a rabbit polyclonal antibody raised against purified StnI. Acid hydrolysis of the proteins (5.7 M HCl for 24 h at 110 °C), followed by the corresponding amino acid analyses made on a Biochrom 20 automatic analyzer (Pharmacia, Pfizer, New York, NY), confirmed the homogeneity of all protein samples used. These results were also used to calculate extinction coefficients for each actinoporin variant (Table 1), which were then employed to calculate protein concentrations in all experiments described below. All the protein batches used were also characterized by recording their far- and near-UV circular dichroism (CD) spectra on a Jasco 715 spectropolarimeter (Easton, MD) and their fluorescence emission spectra on an SLM Aminco model 8000 spectrofluorometer (Urbana, IL), also as previously described [4, 17, 40, 41]. Near and far-UV CD spectra were recorded at 1.0 and 0.2 mg/mL, respectively, in 0.1 M NaCl and 15 mM Mops (pH 7.5). An identical buffer was used for the fluorescence emission spectra with the proteins at concentrations of 0.1 mg/mL. Thermal denaturation was also evaluated as described [31]. At neutral pH, thermal denaturation of Stns occurs simultaneously with a fast aggregation, which can be monitored as optical path clarification (aggregates settling) by CD measurements at 220 nm. Temperature scans were carried out at a rate of 0.5 °C/min. Results are expressed as percentages of the total CD variation versus temperature. T_m corresponds to the temperature at the midpoint of the monophasic transition observed.

Storage stability study

StnIII storage stability was tested by dissolving lyophilized StnIII in 50 mM HCl-Tris pH 7.4, 145 mM NaCl and storing aliquots at 4 °C, -20 °C and -80 °C. Aliquots were analyzed at 24 h, 72 h and one week upon storage and analyzed through 0.1% (w/v) SDS−15% (w/v) PAGE.

Hemolysis assays

Hemolysis assays were performed in 96-multiwell plates as described [4, 6, 31, 35, 37, 41]. Briefly, erythrocytes from heparinized sheep blood were washed in 10 mM HCl-Tris buffer (pH 7.4) containing 0.145 M NaCl, to a final OD_{655} of 0.7 when mixing equal volumes of the cell suspension and buffer. Hemolysis was followed by recording the decrease in OD_{655} after addition of the erythrocyte suspension to different final concentrations of protein. An iMark^{TM} Microplate Absorbance Reader (Bio-Rad, California, USA) was employed to measure OD_{655}.The value obtained with 0.1% (w/v) Na_2CO_3 was considered as 100% hemolysis. HC_{50} values were calculated as the concentration needed to get 50% of hemolysis after 10 minutes of protein addition.

Lipid vesicles preparation

Large unilamelar vesicles (LUVs) of DOPC:SM:Chol (1:1:1) represent one of the membrane models most frequently used to characterize Stns pore formation behavior [4, 6, 11, 17, 26, 31, 35, 41-47]. They were also prepared as described [17, 44-46]. Briefly, a phospholipid (0.1–1.0 mg) solution in 2:1 (v:v) chloroform:methanol was dried under a flow of nitrogen, and the dry film obtained was used to prepare a lipid dispersion by adding 0.5–2.0 mL of HCl-Tris-NaCl buffer (the specific composition depends on the assay developed and is detailed below), briefly vortex mixing, and incubating for 1 h at 37 °C. This suspension of multilamellar vesicles was further subjected to twelve cycles of extrusion at 37 °C through polycarbonate filters (100-nm pore size) (Nucleopore, Whatman) to obtain a homogeneous population of unilamelar vesicles. Aliquots (between 10 and 25 μL) of freshly prepared LUVs were stored to determine the concentration of phospholipids present in the mixture by means of phosphorus quantitation [48].

Calcein leakage assay

Calcein-containing LUVs were also prepared by extrusion through 100 nm filters (Nucleopore, Whatman) at 37 °C [45], essentially as described above but, prior to extrusion, the dry lipid films were hydrated for 1 h at 37 °C in HCl-Tris buffer (10 mM HCl-Tris, 140 mM NaCl, 1 mM EDTA, pH 7.4), containing 100 mM calcein. After hydration, and still before extrusion, the mixture was subjected to 10 freeze/thaw cycles in liquid nitrogen in order to improve calcein encapsulation. LUVs were then extruded, and subsequently separated from non-entrapped calcein by size exclusion chromatography on Sephacryl S200HR column. LUVs were always used for permeabilization studies within the first 24 h after preparation, using 96-multiwell plates and optimized standard protocols [31, 35, 37, 49, 50]. Emission at 520 nm was followed at 25 °C as a function of time (excitation at 485 nm). Fluorescence emission was measured on a FLUOstar OPTIMA microplate reader (BMG-Labtech, Ortenberg, Germany). Two-fold serial dilutions of the proteins were displayed in 96-multiwell plates and after addition of the same volume of calcein-entrapped LUVs (final concentration on the assay was 7.5 μM). Calcein leakage was automatically recorded every 3 s for 250 cycles (total time 12.5 min). One second of shaking was programmed before first measure to ensure the homogeneity within every well. The released fraction of calcein was determined based on the maximal calcein release, which was induced by LUV disintegration in 0.05 % (v/v) Triton X-100 (100% leakage). To ensure that no spontaneous leakage occurred, a 0% leakage control containing buffer and calcein-loaded vesicles was measured through the complete time of the assay. A steady signal level, indicating intact vesicles, was observed for all samples.

Isothermal titration calorimetry

The interaction between actinoporins and LUVs was also quantitated by isothermal titration calorimetry (ITC), as previously described [6, 31, 43, 51], using a VP-ITC calorimeter (Malvern MicroCal Worcestershire, U.K.). Briefly, 0.5–10.0 μM protein solutions were titrated by injection of 20 μL aliquots of lipid suspensions (phospholipid concentration of 0.25–1.0 mM) at a constant temperature of 25 °C. The buffer employed consisted of 10 mM Tris pH 7.4, 100 mM NaCl, and 1 mM EDTA. Binding isotherms were adjusted to a model in which the protein binds to the membrane involving "n" lipid molecules [31].

Results

StnIII purification and sequence differences identification

StnIII was produced in *E. coli* RB791 and purified to homogeneity according to the 0.1% SDS - 15% PAGE analysis of the samples (Figure 3A). Yield of the different purifications was always around 5.0 mg/per liter of original culture broth employed. The amino acid analysis revealed a composition which was consistent with the values expected from the cDNA sequence cloned. This analysis, altogether with the corresponding UV absorption spectrum was also used to calculate an $E^{01\%}$ (280 nm, 1 cm) value of 2.55 (Table 1).

Western blot detection of the purified three *S. helianthus* actinoporins (StnI, II, and III) revealed low immune cross-reactivity of StnIII when assayed against a rabbit polyclonal antibody preparation raised against purified StnI (Figure 3B). On the other hand, and as it was already known [35], StnI and StnII were almost indistinguishable by this analysis, in good agreement with their much higher degree of amino acid sequence identity.

Inspection of Stn I-III's amino acid sequences confirmed that their sequence differences are concentrated along their N-terminal stretches. Also, the N-terminal end of StnIII is 2 and 3 residues longer than the corresponding region in StnI and StnII, respectively (Figure 2) [34]. Another remarkable difference is the presence of a Pro residue at the second position of the StnIII sequence (Figure 2), an amino acid rather incompatible with the formation of an α-helix. These observations should be considered given that previous work shows the N-terminal region of StnII is optimized for spanning a membrane whose bilayer thickness would correspond to vesicles mostly made of di-18:1-PC (DOPC) [26]. StnIII's longer N-terminal stretch, suggests the possibility of different membrane thickness preference for pore formation, thicker in comparison with the optimum value required for StnI and StnII [26].

It has been also shown that an exposed salt bridge between StnI Asp9 and Lys68 explains StnII's higher activity [6]. This difference was attributed to the presence of Ala, instead of Asp, at the corresponding StnII position, a residue with a non-charged and rather hydrophobic sidechain. Interestingly, the corresponding StnIII amino acid is Gln (Figure 2). Gln is also a non-charged residue but still displaying enough negative charge density to be able to interact with the corresponding conserved Lys (Figure 2).

Finally, and within this same N-terminal stretch the hydrophobicity of this region and its hydrophobic moment was *in silico* calculated based on sequence. The hydrophobicity profile calculated for the N-terminal domain of the three known Stns was highly similar (Figure 4A) and followed the same tendency even considering the amino acid variation among them. The hydrophobicity value measures the amphiphilicity of the region and hence its tendency to seek a surface between hydrophobic and hydrophilic phases. It was noticed that the hydrophobicity score [52] of the 30 first residues of StnIII's N-terminal stretch, a critical feature for Stns' cytolytic properties [6], was very similar to the value obtained for StnII [6], therefore higher than the value calculated for StnI (Figure 4B). However, the hydrophobic moment, a magnitude that measures

the affinity for the membrane core [53], was lower than both values calculated for StnI and StnII [6, 23, 25] (Figure 4B), suggesting a lower tendency of this StnIII stretch to cross the membrane. Altogether, all these differences can have profound significance in explaining StnIII activity given the key role played by the stretch comprising the first 30 actinoporins' residues in penetrating the membrane to make a functional pore [6, 19-25].

All the other residues comprising important domains for Stns function [10] are basically conserved or substituted by residues with similar physicochemical properties (Figure 2). The only exception would be Leu113 in StnIII, corresponding to W111 in StnI and W110 in StnII, which stands out because it belongs to the so-called cluster of aromatic residues, responsible for driving membrane binding and involved in maintaining the required hydrophobicity to achieve that goal [41]. According to this observation, in actinoporins where there is not a Trp in this position, there is always Phe or Leu [11], as it is also the case with StnIII.

Spectroscopic characterization

Far-UV CD characterization revealed that the three Stns display very similar spectra (Figure 5A), fully compatible with the canonical actinoporins structural fold [13-18], rich in β-sheet content. Minor differences in the near-UV spectra (Figure 5B) are easily explained by their different aromatic amino acid content (Table 1) and are also in agreement with the adoption of very similar conformational folds. Almost identical conclusions were reached after obtaining the fluorescence emission spectra (Figure 6), being remarkable that the Trp quantum yields are almost identical between StnI and StnIII, despite their different Trp content (Table 1). The most remarkable difference between both StnI and II with StnIII is, however, its much higher Tyr emission quantum yield (Table 1 and Figure 6).

Thermal unfolding analysis (Figure 7) revealed that StnIII was much less thermostable than the other two isotoxins, with a T_m value of 50°C. This value is 15 and 17 °C lower than those obtained for StnI and StnII (Table 1), respectively. Despite this lower thermostability of StnIII, the lyophilized protein remained intact and fully stable for months if stored at -20°C. However, if the protein was maintained in solution, some minor proteolysis was observed. Thus, StnIII aliquots were kept at 4, -20, or -80˚C for 1, 3, or 7 days and then were subjected to 0.1% (w/v) SDS−15% (w/v) PAGE analysis (Figure 8). The results obtained showed a similar behavior for the three different temperatures assayed. StnIII remained intact for at least 72 h and only some degradation was noticed in the samples stored for one week (Figure 8). Therefore, for the functional experiments herein described StnIII was always dissolved in previously autoclaved buffers and only used after storage at 4°C for no more than three days. On the other hand, StnI and II appear fully intact even after one week at room temperature in good agreement with their reported higher thermostability (Table 1).

StnIII functional characterization

Functional characterization of StnIII by hemolysis showed an increased HC_{50} value in comparison with StnI and StnII (Table 1) and, consequently, much less relative hemolytic activity (Table 1). Interestingly, maximum initial rates of hemolysis showed that StnIII was completely inactive at concentration values below 10 nM (Figure 9) but, upon reaching the critical value of 20 nM, StnIII was significantly faster than StnI at comparable concentrations (Figure 9). This stronger concentration dependence is probably related to the oligomerization step of the pore formation mechanism. Equivalent results were observed when calcein release from DOPC:SM:Chol (1:1:1) vesicles was evaluated (Figure 10). Both the effects of StnI and StnIII were negligible below 10 nM but, once reaching that critical concentration value, the maximal rate of calcein release was increased for both proteins, being this increment sharper for StnIII (Figure 10).

Membrane binding affinity of StnIII to these model membranes was calculated by ITC (Figure 11). The thermodynamic parameters obtained after analysis of the thermograms are summarized in Table 2. StnIII membrane binding affinity for the DOPC:SM:Chol (1:1:1) model vesicles was only a marginally smaller than for StnI, as revealed by their RMB values (Table 2), but almost seven-fold lower when compared to StnII (Table 2). Another significant difference was the smaller number of lipid molecules affected by StnIII binding when compared to the values obtained for the other two Stns known (Table 2). This fact, in combination with the lower membrane binding affinity, could be related to the necessity of a higher StnIII concentration for erythrocytes or model vesicles disruption and suggests a different mechanism of action. All these results would agree with those from the hemolysis and calcein leakage experiments.

Discussion

Considering the multigenic character of the sticholysin's family [1, 3, 5], it was hypothesized that small amounts of other Stns, not yet detected, might also be produced by *S. helianthus* to further expand whole venom versatility. Transcriptomic profiling was performed as an effective approach for discovering new toxins produced by this sea anemone [34]. It was concluded that *S. helianthus* produces at least one more actinoporin isoform, which was designated as StnIII. The phylogenetic analysis revealed that it was more closely related to other species' actinoporins rather than to the other well-studied isotoxins produced by *S. helianthus*. StnIII's lower sequence conservation was fully compatible with the small cross-reactivity observed in Western blot experiments (Figure 3B), and still high enough to allow a faithful prediction of StnIII's three-dimensional structure which resulted in a conformation perfectly compatible with the very well-known actinoporins' common fold [15, 17] and their far-UV CD spectra (Figure 5). Nevertheless, amino acid sequence comparison among the three proteins showed significant differences, especially at their N-terminal stretch (Figure 1).

The StnIII N-terminal sequence is 2 and 3 residues longer than the corresponding region in StnI and StnII, respectively, and a particularly interesting detail is that the second residue of this region is a Pro, an imino acid that, although participating in extended protein segments, would not easily incorporate into a full α-helical structure when spanning the hydrophobic core of the membrane in order to constitute a pore (Figure 2). In addition, the hydrophobicity of this sequence stretch was also lower, suggesting a minor tendency to cross the membrane [6, 26, 34] and maybe explaining its lower hemolytic activity (Figure 9).

The observation that the N-terminal end of StnIII is three residues longer than this same stretch in StnII is relevant because it has been shown that bilayer thickness affects both functional and conformational aspects of Stns membrane binding and pore formation [26]. Accordingly, the length of the StnII N-terminal α-helix, which penetrates the membrane to form a functional pore, appeared to be optimal for the membrane thickness represented by DOPC. Applying identical geometrical calculations to StnIII, the α-helical transmembrane domain would be 49.5 Å long, instead of the 45.0 Å calculated for StnII [26]. Assuming a final pore octameric stoichiometry identical to the one found for the actinoporin from *Actinia fragacea*, FraC [18], and taking into account the angle formed by the helix and the bilayer normal, the optimal thickness for StnIII would be 42.5 Å, instead of the 38.0 Å described for StnII [26]. This membrane thickness would correspond 1,2-dieicosenoyl-sn-glycero-3-phosphocholine (di-20:1-PC), suggesting that StnIII's presence in *S. helianthus* venom could represent the possibility of targeting cells with thicker membranes than the most common ones found in fishes, containing di-18:1-PC as its major phospholipid [54]. Another possibility to explain StnIII's longer N-terminal end would be maintaining the di-18:1-PC membrane thickness but adopting a different stoichiometry for its final stable pore. Interestingly, a nonameric structure has been also described for FraC [16].

Finally, the presence of Pro in the second position also opens the possibility that StnIII uses a slightly different conformation, other than a 100% α-helix, to penetrate the membrane.

All the other residues comprising important domains for the actinoporins function [10] are conserved or substituted by residues with similar physicochemical properties (Figure 1) [41]. Within this context, StnIII L113, corresponding to W111 in StnI and W110 in StnII, stands out because this residue belongs to the so-called cluster of aromatic residues, responsible for driving membrane binding and involved in maintaining the required hydrophobicity to achieve that goal. In agreement with this observation, StnII W110 has been recently described as penetrating the hydrophobic membrane core [41]. In fact, its substitution by another highly hydrophobic amino acid such as Phe barely affected membrane binding [41]. Accordingly, substitution by another highly hydrophobic amino acid, as is the case with L113, would be expected to have only minor influence on StnIII membrane interaction ability, as occurs with some other less studied actinoporins [11].

As stated above, StnIII is a sticholysin with only four Trp residues, instead of five as in the other two. The role played by the different StnII Trp residues has been previously analyzed in detail using a quite complete set of Trp to Phe mutants [41]. Apart from its role in membrane binding, in its monomeric water-soluble conformation StnII W110 is a fully exposed residue that does not contribute significantly to fluorescence emission, explaining why its substitution by Leu in StnIII does not involve major significant differences in terms of Trp fluorescence emission, when compared to StnII (Figure 6; Table 1), despite of having one less Trp residue [55].

On the other hand, the most remarkable feature that emerges from Figure 6 is the relatively much higher Tyr quantum yield. For example, StnIII's Tyr emission is about four-fold higher than StnII's (Table 1), for example). An observation that is even more noticeable considering that StnI and StnII contain 13 and 12 Tyr residues, respectively, while StnIII contains only 11. García-Linares et al. [41] found that replacement of W110 (the StnII equivalent residue of StnIII L113; Figure 1B) yielded mutants showing a significant increase in Tyr emission. This was interpreted as StnII Y114 being quenched through non-radiative energy transfer to StnII W110. This non-radiative energy transfer phenomenon could not take place in StnIII due to the presence of Leu in that critical position (Figure 1B), possibly explaining the high Tyr quantum yield increment observed (Figure 6).

Finally, comparison between StnII and StnIII sequences reveals that StnII Y140 is in a position equivalent to StnIII F143 (Figures 1 and 2). StnII Y140 seems to be quenched by W115 (Figure 1C) supporting another event of non-radiative energy transfer between Tyr and Trp residues [41]. This interpretation explains why Y140 does not contribute significantly to StnII fluorescence emission [41]. Consequently, the change of this residue by Phe in the equivalent position of StnIII has a negligible effect on the StnIII fluorescence emission while Phe is still an amino acid with the properties needed to establish the required stabilizing interaction with StnIII W118 (Figure 1C).

StnI and III showed very similar relative binding affinity values (Table 2) but StnIII's relative hemolytic activity was four-fold lower (Table 1). Both proteins are significantly much less efficient than StnII in terms of membrane binding and lytic activity (Tables 1 and 2). These results suggest that StnI and StnIII functional differences would reside rather on the membrane diffusion and oligomerization steps needed to form the final pore than on their ability to recognize and bind to the membrane surface. Accordingly, inspection of their hemolytic behavior in kinetic terms reveals that both hemolytic curves of StnI and III (Figure 9) are quite different. Apparently, the critical concentration for StnIII to become hemolytic is higher in comparison with StnI but, once reached, StnIII displays higher activity than StnI. This observation agrees with the interpretation that both proteins would mostly differ in their oligomerization mechanism. Furthermore, it could

also be speculated that it agrees with the above mentioned hypothesis that the final pore assembly of StnIII might display a different stoichiometry other than an octamer, as described for the pore crystalline structure of FraC [18].

Conclusions

StnIII is a new actinoporin isoform produced by *S. helianthus*, discovered through transcriptomic analysis. This protein has been cloned and produced in the heterologous system *E. coli*. Its successful purification allowed its spectroscopic and functional characterization. Its spectroscopic features are compatible with the protein adopting a globular β-sheet rich conformation that would resemble the common actinoporin fold. StnIII is active against sheep red blood cells, but significantly less hemolytic than StnII and quite similar to StnI in spite of its much higher HC_{50} value which, in this case, could be attributed to a different oligomerization behavior on the membrane rather than to a less hemolytic efficiency. This behavior was also consistent with the calcein release and model membranes binding experiments. The results, altogether with its longer N-terminal end and the presence of Pro as its second amino acid, suggest the possibility of StnIII oligomerizing into a final membrane structure whose stoichiometry would be larger. The results shown reinforce the hypothesis that the presence of different actinoporin isoforms plays a key role in expanding the range of targets the venom can act against.

Acknowledgements

This research was supported by the Sigrid Juselius Foundation, the Jane and Aatos Erkko Foundation, and the Magnus Ehrnrooth Foundation (to J.P.S.), and by UCM-Banco Santander grant PR75/18-21561 (to A.M.-d.-P.). J.P.-O. has a funded doctoral student position from ISB/ÅA. UCM-Banco Santander fellowship was granted to E.R.-d.-T.

References

[1] Y. Wang, L.L. Yap, K.L. Chua, H.E. Khoo, A multigene family of *Heteractis* magnificalysins (HMgs), Toxicon 51(8) (2008) 1374-1382.

[2] M. Monastyrnaya, E. Leychenko, M. Isaeva, G. Likhatskaya, E. Zelepuga, E. Kostina, E. Trifonov, E. Nurminski, E. Kozlovskaya, Actinoporins from the sea anemones, tropical *Radianthus macrodactylus* and northern *Oulactis orientalis*: Comparative analysis of structure-function relationships, Toxicon 56(8) (2010) 1299-1314.

[3] J. Macrander, M. Daly, Evolution of the Cytolytic Pore-Forming Proteins (Actinoporins) in Sea Anemones, Toxins (Basel) 8(12) (2016).

[4] S. García-Linares, E. Rivera-de-Torre, K. Morante, K. Tsumoto, J.M. Caaveiro, J.G. Gavilanes, J.P. Slotte, Á. Martínez-del-Pozo, Differential effect of membrane composition on the pore-forming ability of four different sea anemone actinoporins, Biochemistry 55(48) (2016) 6630-6641.

[5] E.V. Leychenko, M. Isaeva, E. Tkacheva, E. Zelepuga, A. Kvetkina, K. Guzev, M. Monastyrnaya, E. Kozlovskaya, Multigene family of pore-forming toxins from sea anemone *Heteractis crispa*, Mar Drugs 16(6) (2018).

[6] E. Rivera-de-Torre, J. Palacios-Ortega, S. García-Linares, J.G. Gavilanes, A. Martínez-del-Pozo, One single salt bridge explains the different cytolytic activities shown by actinoporins sticholysin I and II from the venom of *Stichodactyla helianthus*, Arch Biochem Biophys 636 (2017) 79-89.

[7] M.W. Parker, S.C. Feil, Pore-forming protein toxins: from structure to function, Prog Biophys Mol Biol 88(1) (2005) 91-142.

[8] G. Anderluh, J.H. Lakey, Disparate proteins use similar architectures to damage membranes, Trends Biochem Sci 33(10) (2008) 482-90.

[9] G. Anderluh, P. Maček, Cytolytic peptide and protein toxins from sea anemones (Anthozoa: Actiniaria), Toxicon 40(2) (2002) 111-24.

[10] L. García-Ortega, J. Alegre-Cebollada, S. García-Linares, M. Bruix, A. Martínez-del-Pozo, J.G. Gavilanes, The behavior of sea anemone actinoporins at the water-membrane interface, Biochim Biophys Acta 1808(9) (2011) 2275-88.

[11] S. García-Linares, E. Rivera-de-Torre, J. Palacios-Ortega, J.G. Gavilanes, A. Martínez-del-Pozo, The metamorphic transformation of a water-soluble monomeric protein into an oligomeric transmembrane pore, in: A. Iglič, M. Rappolt, A.J. García-Sáez (Eds.), Advances in Biomembranes and Lipid Self-Assembly2017, pp. 51-97.

[12] J. Alegre-Cebollada, M. Oñaderra, J.G. Gavilanes, A. Martínez-del-Pozo, Sea anemone actinoporins: The transition from a folded soluble state to a functionally active membrane-bound oligomeric pore, Curr Protein Pept Sci 8(6) (2007) 558-72.

[13] A. Athanasiadis, G. Anderluh, P. Maček, D. Turk, Crystal structure of the soluble form of equinatoxin II, a pore-forming toxin from the sea anemone *Actinia equina*, Structure 9(4) (2001) 341-6.

[14] M.G. Hinds, W. Zhang, G. Anderluh, P.E. Hansen, R.S. Norton, Solution structure of the eukaryotic pore-forming cytolysin equinatoxin II: Implications for pore formation, J Mol Biol 315(5) (2002) 1219-1229.

[15] J.M. Mancheño, J. Martín-Benito, M. Martínez-Ripoll, J.G. Gavilanes, J.A. Hermoso, Crystal and electron microscopy structures of sticholysin II actinoporin reveal insights into the mechanism of membrane pore formation, Structure 11(11) (2003) 1319-1328.

[16] A.E. Mechaly, A. Bellomio, D. Gil-Carton, K. Morante, M. Valle, J.M. González-Mañas, D.M. Guerin, Structural insights into the oligomerization and architecture of eukaryotic membrane pore-forming toxins, Structure 19(2) (2011) 181-91.

[17] S. García-Linares, I. Castrillo, M. Bruix, M. Menéndez, J. Alegre-Cebollada, A. Martínez-del-Pozo, J.G. Gavilanes, Three-dimensional structure of the actinoporin sticholysin I. Influence of long-distance effects on protein function, Arch Biochem Biophys 532(1) (2013) 39-45.

[18] K. Tanaka, J.M. Caaveiro, K. Morante, J.M. González-Mañas, K. Tsumoto, Structural basis for self-assembly of a cytolytic pore lined by protein and lipid, Nat Commun 6 (2015) 6337.

[19] F. Casallanovo, F.J.F. de Oliveira, A.L.C.F. Souto, F.C. de Souza, E.M. Cilli, Y. Martínez, M.E. Lanio, C. Álvarez, Peptides from the N-terminal domain of a pore-forming toxin, Sticholysin II. Conformation and activity., 48th Annual Meeting of the Biophysical Society, Biophysical Journal, Baltimore, MD, 2004.

[20] F. Casallanovo, F.J. de Oliveira, F.C. de Souza, U. Ros, Y. Martínez, D. Penton, M. Tejuca, D. Martínez, F. Pazos, T.A. Pertinhez, A. Spisni, E.M. Cilli, M.E. Lanio, C. Álvarez, S. Schreier, Model peptides mimic the structure and function of the N-terminus of the pore-forming toxin sticholysin II, Biopolymers 84(2) (2006) 169-80.

[21] E.M. Cilli, F.T. Pigossi, E. Crusca, Jr., U. Ros, D. Martinez, M.E. Lanio, C. Alvarez, S. Schreier, Correlations between differences in amino-terminal sequences and different hemolytic activity of sticholysins, Toxicon (2007).

[22] I. Castrillo, N.A. Araujo, J. Alegre-Cebollada, J.G. Gavilanes, A. Martínez-del-Pozo, M. Bruix, Specific interactions of sticholysin I with model membranes: an NMR study, Proteins 78(8) (2010) 1959-70.

[23] U. Ros, L. Pedrera, D. Diaz, J.C. Karam, T.P. Sudbrack, P.A. Valiente, D. MartInez, E.M. Cilli, F. Pazos, R. Itri, M.E. Lanio, S. Schreier, C. Avarez, The membranotropic activity of N-terminal peptides from the pore-forming proteins sticholysin I and II is modulated by hydrophobic and electrostatic interactions as well as lipid composition, J Biosci 36(5) (2012) 781-91.

[24] N. Rojko, K.C. Kristan, G. Viero, E. Zerovnik, P. Maček, M. Dalla Serra, G. Anderluh, Membrane damage by an α-helical pore-forming protein, Equinatoxin II, proceeds through a succession of ordered steps, J Biol Chem 288(33) (2013) 23704-15.

[25] U. Ros, W. Rodríguez-Vera, L. Pedrera, P.A. Valiente, S. Cabezas, M.E. Lanio, A.J. García-Saez, C. Álvarez, Differences in activity of actinoporins are related with the hydrophobicity of their N-terminus, Biochimie 116 (2015) 70-8.

[26] J. Palacios-Ortega, S. García-Linares, E. Rivera-de-Torre, J.G. Gavilanes, A. Martínez-del-Pozo, J.P. Slotte, Differential Effect of Bilayer Thickness on Sticholysin Activity, Langmuir 33(41) (2017) 11018-11027.

[27] Q. Hong, I. Gutiérrez-Aguirre, A. Barlič, P. Malovrh, K. Kristan, Z. Podlesek, P. Maček, D. Turk, J.M. González-Mañas, J.H. Lakey, G. Anderluh, Two-step Membrane Binding by Equinatoxin II, a Pore-forming Toxin from the Sea Anemone, Involves an Exposed Aromatic Cluster and a Flexible Helix, J Biol Chem 277(44) (2002) 41916-41924.

[28] P. Malovrh, G. Viero, M.D. Serra, Z. Podlesek, J.H. Lakey, P. Maček, G. Menestrina, G. Anderluh, A novel mechanism of pore formation: membrane penetration by the N-terminal amphipathic region of equinatoxin, J Biol Chem 278(25) (2003) 22678-85.

[29] K. Kristan, Z. Podlesek, V. Hojnik, I. Gutiérrez-Aguirre, G. Guncar, D. Turk, J.M. González-Mañas, J.H. Lakey, P. Maček, G. Anderluh, Pore Formation by Equinatoxin, a Eukaryotic Pore-forming Toxin, Requires a Flexible N-terminal Region and a Stable β-Sandwich, J Biol Chem 279(45) (2004) 46509-46517.

[30] J. Alegre-Cebollada, A. Martínez-del-Pozo, J.G. Gavilanes, E. Goormaghtigh, Infrared spectroscopy study on the conformational changes leading to pore formation of the toxin sticholysin II, Biophys J 93(9) (2007) 3191-201.

[31] J. Alegre-Cebollada, M. Cunietti, E. Herrero-Galán, J.G. Gavilanes, A. Martínez-del-Pozo, Calorimetric scrutiny of lipid binding by sticholysin II toxin mutants, J Mol Biol 382(4) (2008) 920-30.

[32] N. Rojko, M. Dalla Serra, P. Maček, G. Anderluh, Pore formation by actinoporins, cytolysins from sea anemones, Biochim Biophys Acta 1858(3) (2016) 446-56.

[33] M.E. Lanio, V. Morera, C. Álvarez, M. Tejuca, T. Gómez, F. Pazos, V. Besada, D. Martínez, V. Huerta, G. Padrón, M.A. Chavez, Purification and characterization of two hemolysins from *Stichodactyla helianthus*, Toxicon 39(2-3) (2001) 187-194.

[34] E. Rivera-de-Torre, A. Martínez-del-Pozo, J.E. Garb, *Stichodactyla helianthus*' de novo transcriptome assembly: Discovery of a new actinoporin isoform, Toxicon 150 (2018) 105-114.

[35] E. Rivera-de-Torre, S. García-Linares, J. Alegre-Cebollada, J. Lacadena, J.G. Gavilanes, A. Martínez-del-Pozo, Synergistic Action of Actinoporin Isoforms from the Same Sea Anemone Species Assembled into Functionally Active Heteropores, J Biol Chem 291(27) (2016) 14109-19.

[36] V. De los Ríos, M. Oñaderra, A. Martínez-Ruiz, J. Lacadena, J.M. Mancheño, A. Martínez-del-Pozo, J.G. Gavilanes, Overproduction in *Escherichia coli* and purification of the hemolytic protein sticholysin II from the sea anemone *Stichodactyla helianthus*, Protein Expr Purif 18(1) (2000) 71-6.

[37] J. Alegre-Cebollada, G. Clementi, M. Cunietti, C. Porres, M. Oñaderra, J.G. Gavilanes, A. Martínez-del-Pozo, Silent mutations at the 5'-end of the cDNA of actinoporins from the sea anemone *Stichodactyla helianthus* allow their heterologous overproduction in *Escherichia coli*, J Biotechnol 127(2) (2007) 211-21.

[38] U.K. Laemli, Cleavage of structural proteins during the assembly of the head of bacteriophage T4, Nature 227 (1970) 680-685.

[39] A. Martínez-Ruiz, L. García-Ortega, R. Kao, M. Oñaderra, J.M. Mancheño, J. Davies, A. Martínez-del-Pozo, J.G. Gavilanes, Ribonuclease U2: cloning, production in *Pichia pastoris* and

affinity chromatography purification of the active recombinant protein, FEMS Microbiol Lett 189(2) (2000) 165-9.

[40] C. De Antonio, A. Martínez-del-Pozo, J.M. Mancheño, M. Oñaderra, J. Lacadena, A. Martínez-Ruiz, J.M. Pérez-Cañadillas, M. Bruix, J.G. Gavilanes, Assignment of the contribution of the tryptophan residues to the spectroscopic and functional properties of the ribotoxin α-sarcin, Proteins 41(3) (2000) 350-61.

[41] S. García-Linares, T. Maula, E. Rivera-de-Torre, J.G. Gavilanes, J.P. Slotte, A. Martínez-del-Pozo, Role of the tryptophan residues in the specific interaction of the sea anemone *Stichodactyla helianthus*'s actinoporin sticholysin II with biological membranes, Biochemistry 55(46) (2016) 6406-6420.

[42] J. Alegre-Cebollada, I. Rodríguez-Crespo, J.G. Gavilanes, A. Martínez-del-Pozo, Detergent-resistant membranes are platforms for actinoporin pore-forming activity on intact cells, FEBS J 273(4) (2006) 863-71.

[43] S. García-Linares, R. Richmond, M.F. García-Mayoral, N. Bustamante, M. Bruix, J.G. Gavilanes, A. Martínez-del-Pozo, The sea anemone actinoporin (Arg-Gly-Asp) conserved motif is involved in maintaining the competent oligomerization state of these pore-forming toxins, FEBS J 281(5) (2014) 1465-78.

[44] S. García-Linares, I. Alm, T. Maula, J.G. Gavilanes, J.P. Slotte, A. Martínez-Del-Pozo, The effect of cholesterol on the long-range network of interactions established among sea anemone Sticholysin II residues at the water-membrane interface, Mar Drugs 13(4) (2015) 1647-65.

[45] S. García-Linares, J. Palacios-Ortega, T. Yasuda, M. Astrand, J.G. Gavilanes, A. Martínez-del-Pozo, J.P. Slotte, Toxin-induced pore formation is hindered by intermolecular hydrogen bonding in sphingomyelin bilayers, Biochim Biophys Acta 1858(6) (2016) 1189-95.

[46] J. Palacios-Ortega, S. García-Linares, M. Astrand, M.A. Al Sazzad, J.G. Gavilanes, A. Martínez-del-Pozo, J.P. Slotte, Regulation of Sticholysin II-Induced Pore Formation by Lipid Bilayer Composition, Phase State, and Interfacial Properties, Langmuir 32(14) (2016) 3476-84.

[47] J. Palacios-Ortega, S. García-Linares, E. Rivera-de-Torre, J.G. Gavilanes, A. Martínez-del-Pozo, J.P. Slotte, Sticholysin, Sphingomyelin, and Cholesterol: A Closer Look at a Tripartite Interaction, Biophys J 116(12) (2019) 2253-2265.

[48] G.R. Bartlett, Colorimetric assay methods for free and phosphorylated glyceric acids, J Biol Chem 234(3) (1959) 469-71.

[49] V. De los Ríos, J.M. Mancheño, M.E. Lanio, M. Oñaderra, J.G. Gavilanes, Mechanism of the leakage induced on lipid model membranes by the hemolytic protein sticholysin II from the sea anemone *Stichodactyla helianthus*, Eur J Biochem 252 (1998) 284-289.

[50] J. Alegre-Cebollada, V. Lacadena, M. Oñaderra, J.M. Mancheño, J.G. Gavilanes, A. Martínez-del-Pozo, Phenotypic selection and characterization of randomly produced non-

haemolytic mutants of the toxic sea anemone protein sticholysin II, FEBS Lett 575(1-3) (2004) 14-8.

[51] T. Maula, Y.J. Isaksson, S. García-Linares, S. Niinivehmas, O.T. Pentikainen, M. Kurita, S. Yamaguchi, T. Yamamoto, S. Katsumura, J.G. Gavilanes, A. Martínez-del-Pozo, J.P. Slotte, 2NH and 3OH are crucial structural requirements in sphingomyelin for sticholysin II binding and pore formation in bilayer membranes, Biochim Biophys Acta 1828(5) (2013) 1390-5.

[52] J. Kyte, R.F. Doolittle, A simple method for displaying the hydropathic character of a protein, J Mol Biol 157(1) (1982) 105-32.

[53] D. Eisenberg, E. Schwarz, M. Komaromy, R. Wall, Analysis of membrane and surface protein sequences with the hydrophobic moment plot, J Mol Biol 179 (1984) 125-142.

[54] G. Li, A.J. Sinclair, D. Li, Comparison of lipid content and Fatty Acid composition in the edible meat of wild and cultured freshwater and marine fish and shrimps from china, J Agric Food Chem 59(5) (2011) 1871-81.

[55] B. Bakrač, I. Gutierrez-Aguirre, Z. Podlesek, A.F. Sonnen, R.J. Gilbert, P. Maček, J.H. Lakey, G. Anderluh, Molecular determinants of sphingomyelin specificity of a eukaryotic pore-forming toxin, J Biol Chem 283(27) (2008) 18665-77.

[56] L.A. Kelley, S. Mezulis, C.M. Yates, M.N. Wass, M.J. Sternberg, The Phyre2 web portal for protein modeling, prediction and analysis, Nat Protoc 10(6) (2015) 845-58.

[57] R. Gautier, D. Douguet, B. Antonny, G. Drin, HELIQUEST: a web server to screen sequences with specific alpha-helical properties, Bioinformatics 24(18) (2008) 2101-2.

Tables

Table 1. Calculated extinction coefficients ($E^{0.1\%}$), content of Trp and Tyr residues, relative Trp and Tyr emission yields, and melting temperature (T_m), and HC_{50}, values of the three Stn natural variants used in this study.

	$E^{0.1\%}$ (280 nm, 1 cm)	Number of Trp	Number of Tyr	Relative Trp emission yield[a]	Relative Tyr emission yield[a]	T_m (°C)	HC_{50} (nM)
StnI	2.55[b]	5	13	1.00	1.00	65.0 ± 0.1[b]	3.0[c]
StnII	2.54[b]	5	12	1.22	2.11	67.0 ± 0.1[b]	0.4[c]
StnIII	2.55	4	11	0.96	9.14	50.0 ± 0.2	12.0

[a]Calculated as the area corresponding to the Trp or Tyr emission spectra of each protein (Figure 6) referred to the StnI emission [4, 41]
[b]Calculated in [4, 31]

Table 2. Binding to DOPC:SM:Chol (1:1:1) vesicles by StnI, II and III studied by ITC. All results shown are the average of at least three independent experiments.

	n	K_b ($x10^{-6}$ M^{-1})	ΔG (kcal/mol)	ΔH (kcal/mol)	ΔS (cal mol^{-1} K^{-1})	RMB[a]
StnI[b]	49 ± 4	0.41 ± 0.03	-8.21 ± 0.03	-20.9 ± 2.1	-42.84 ± 6.78	1.00
StnII[b]	39 ± 4	1.70 ± 0.90	-9.10 ± 0.50	-44.0 ± 3.0	-115.00 ± 9.00	5.21
StnIII	26 ± 1	0.17 ± 0.40	-7.41 ± 0.22	-7.85 ± 0.31	-4.59 ± 1.78	0.78

[a]Relative membrane binding values calculated according to [n(StnI) × K_b(other actinoporin)]/[n(other actinoporin) × K_b(StnI)] as explained in [31].
[b]As reported before [31, 35]

Figures

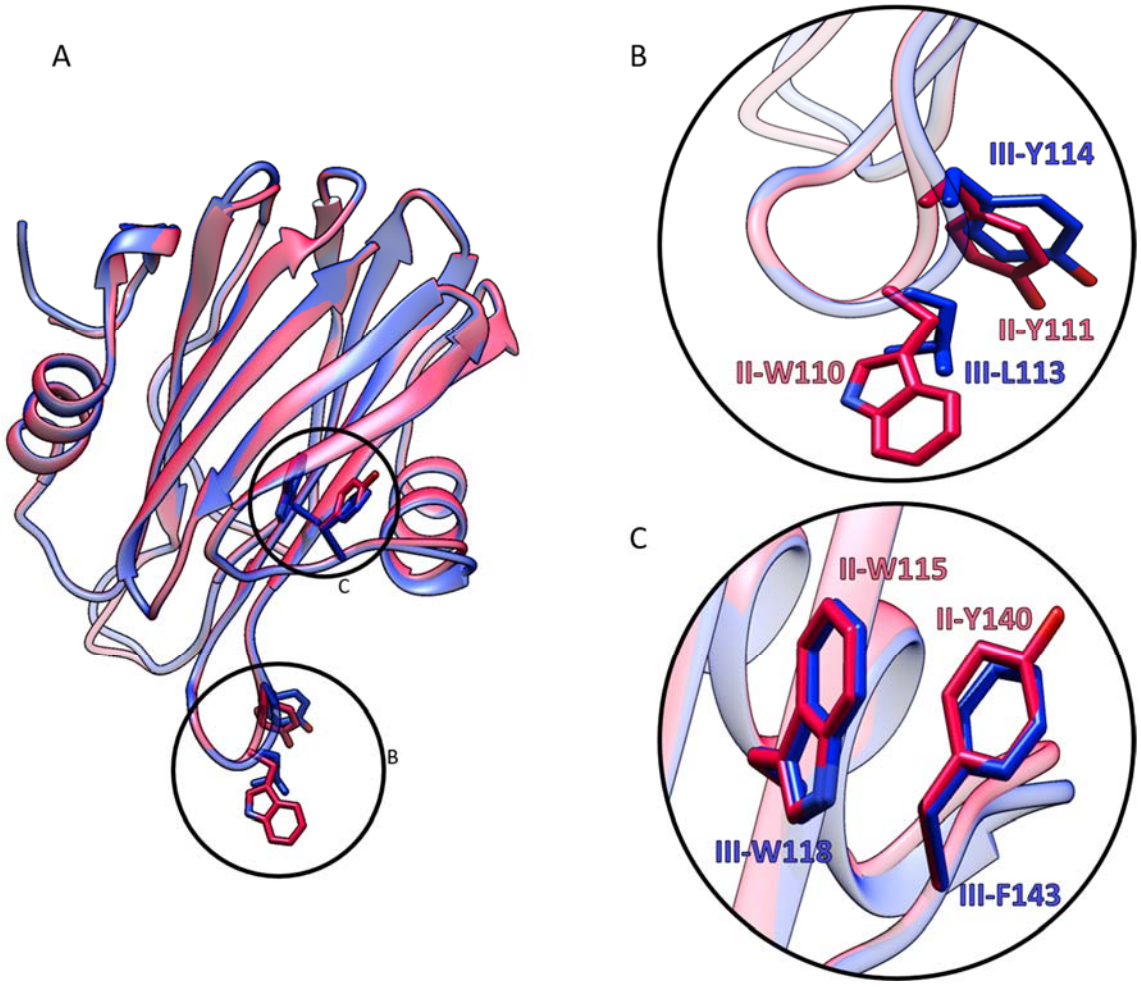

Figure 1. (A) StnII (pink, PDB: 1GWY) and StnIII (blue, predicted structure with Phyre2 [56]) aligned three-dimensional structures. Circles indicate the close-up views. (B) Close-up showing the relative positions of StnII W110 and Y111 (pink), StnIII L113 and Y114 (blue). (C) Close-up of the three-dimensional structure showing the relative positions of StnII Y140 and StnII W115 (pink), StnIII F143 and W118 (blue).

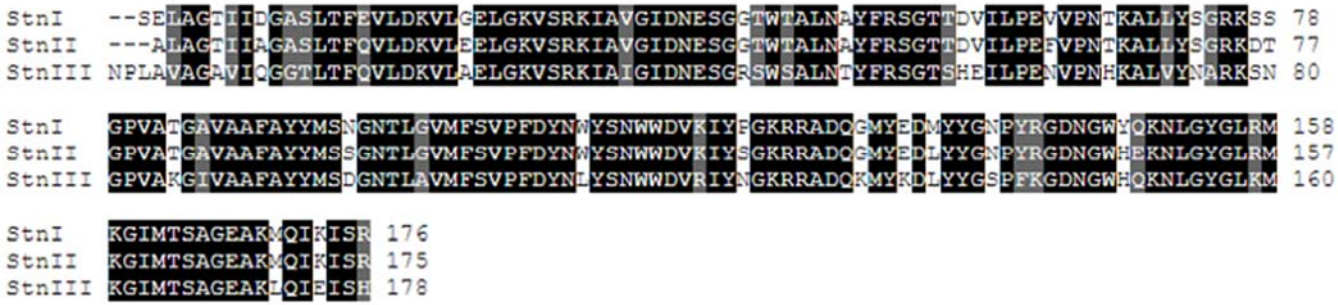

Figure 2. Sequence alignment of the three Stns produced by *S. helianthus*. Black background indicates conservation of the same amino acid while grey is for conservative substitutions.

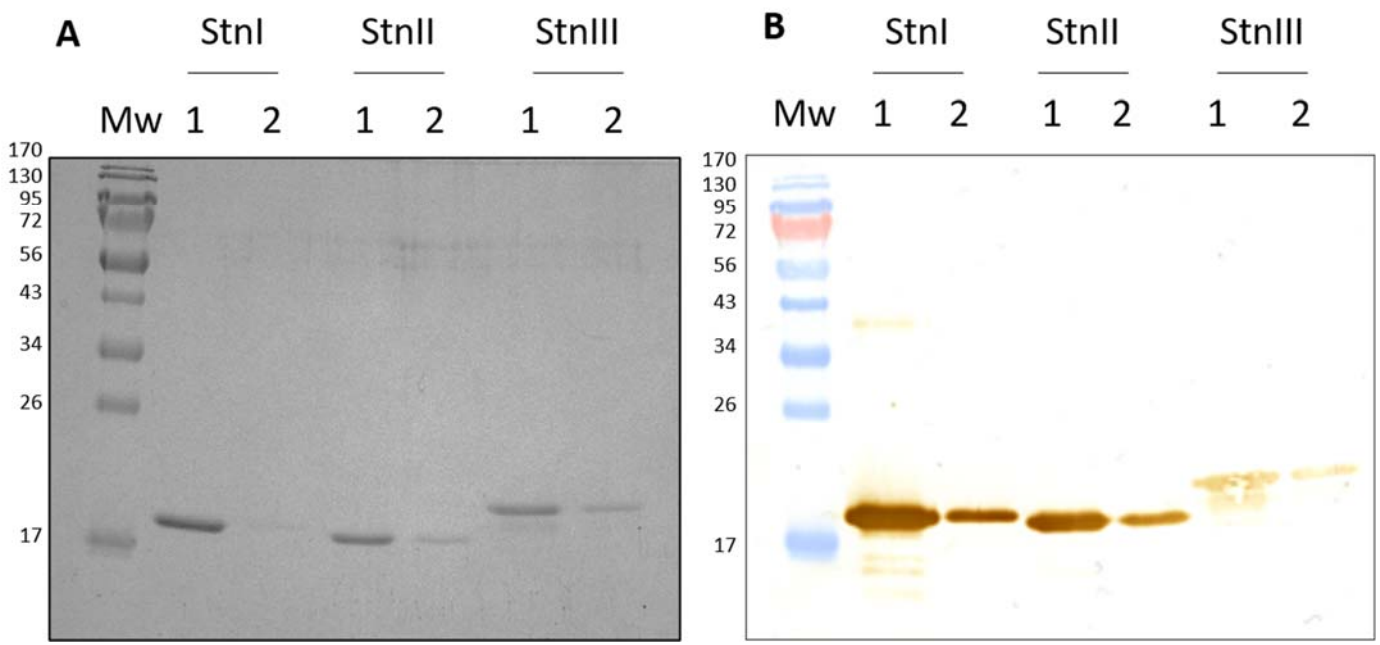

Figure 3. Electrophoretic and western blot analysis of the purified proteins. (Mw) Molecular weight standard (EZ-RUNTM pre-stained Rec Protein Ladder – Fisher Scientific) were also loaded, and the corresponding molecular masses are indicated in kDa at the left margin. (1) 0.5 µg and (2) 0.1 µg of StnI, StnII or StnIII, as indicated. (A) 0.1% SDS - 15% PAGE analysis of the three purified sticholysin natural variants. (B) Western Blot using a rabbit polyclonal serum raised against StnI.

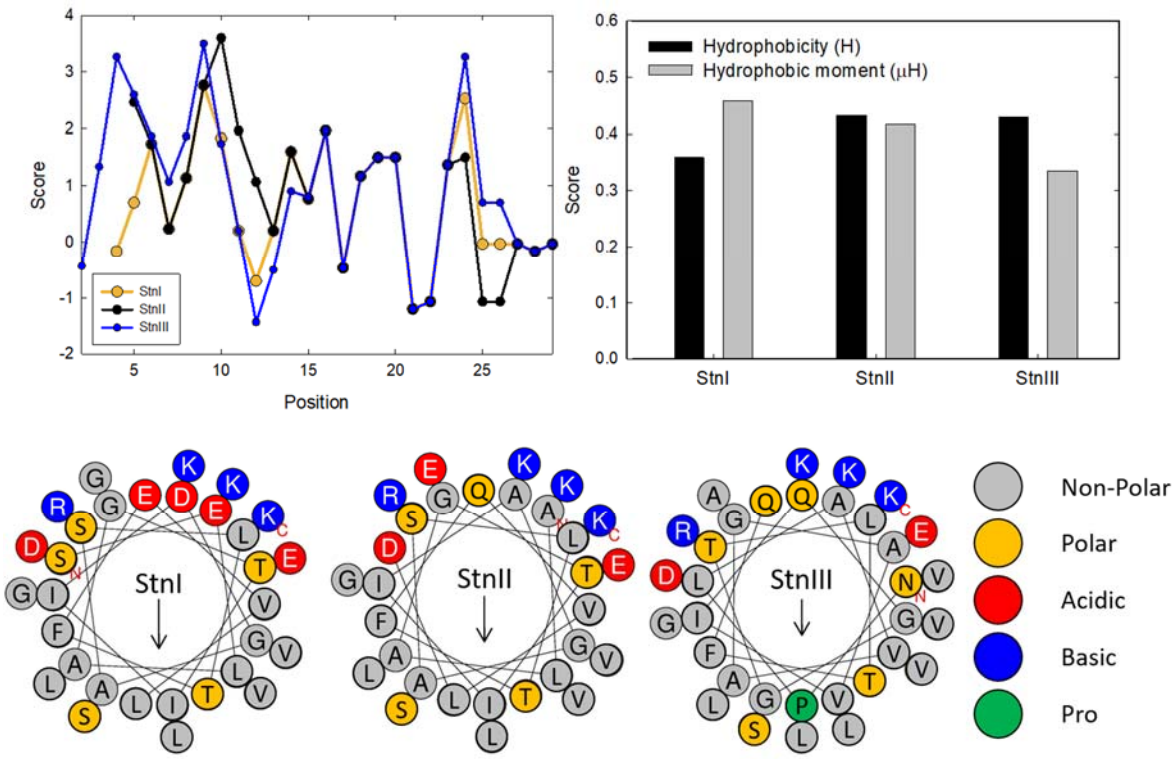

Figure 4. Hydrophobicity profile of Stns' N-terminal ends [52] (A), calculated hydrophobicity (H) [53] and hydrophobic moment (μH) [53] (B) of the first 31, 30 and 33 residues of StnI, II and III respectively. The window size employed in (A) was 3 amino acids and the graph was made through simulation at Expasy ProScale web server tool (http://web.expasy.org/protscale/). (C) Helical wheel representation of the same Stns N-terminal amino acid residues. The arrow module indicates the hydrophobic moment and the direction marks the most hydrophobic face of the α-helix. N-termini and C-termini are indicated in red. Analysis were performed using the web server HELIQUEST [57].

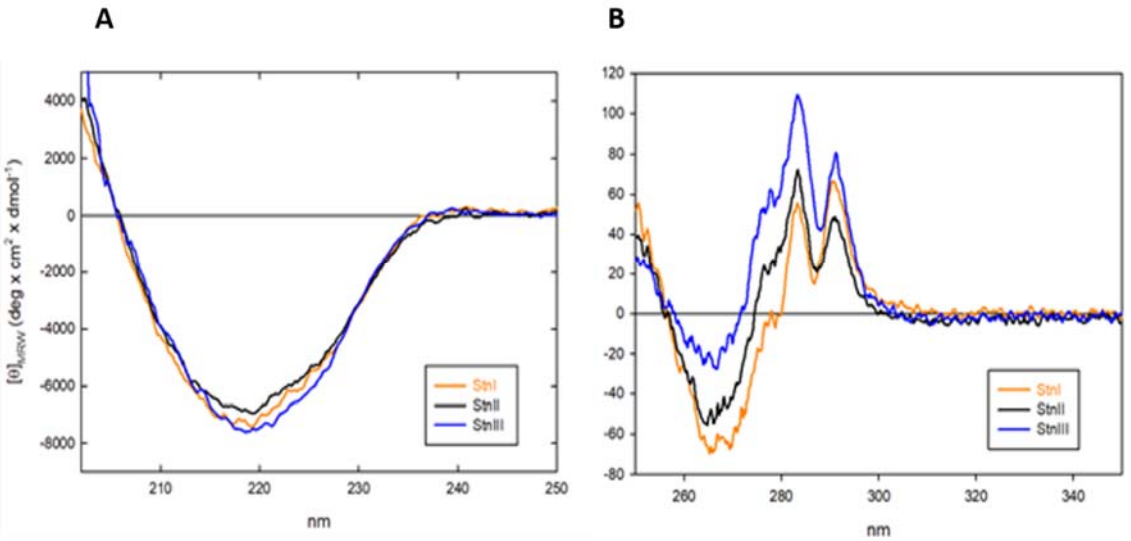

Figure 5. Circular dichroism spectra of the three purified Stns. (A) Far- and (B) near-UV spectra of StnI (orange line), StnII (black line), and StnIII (blue line).

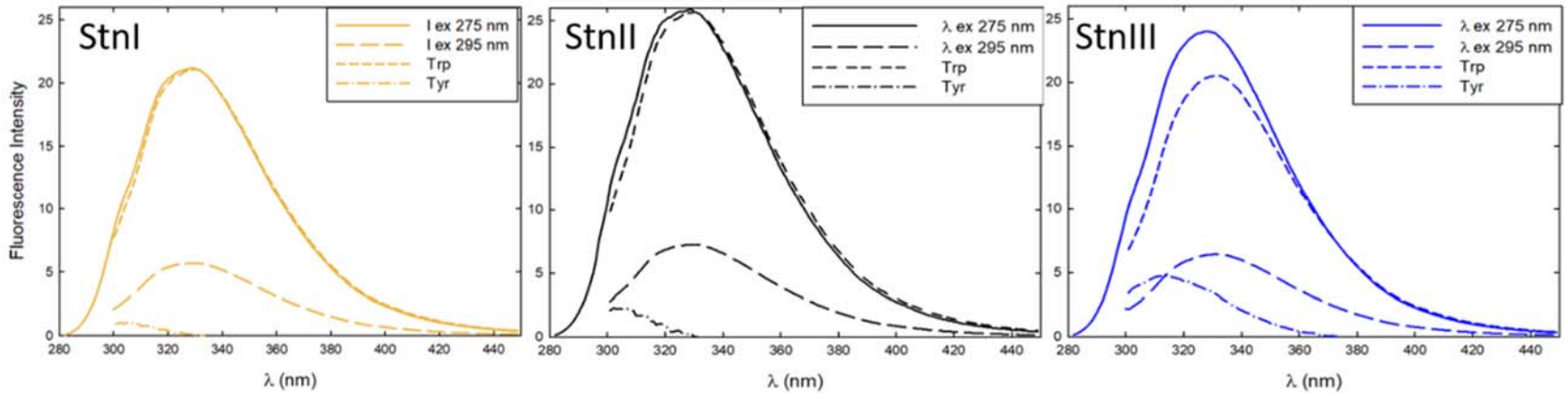

Figure 6. Fluorescence emission spectra of the three Stns produced by *S. helianthus*. StnI (orange), StnII (black), and StnIII (blue). All spectra were recorded at identical protein concentrations of 0.1 mg/mL. Experimental spectra resulted from excitation at 275 nm (solid lines) and 295 nm (long dashed lines). These spectra obtained upon excitation at 295 nm were normalized at wavelengths above 380 nm to obtain the Trp contributions (short dashed bold lines). Tyr contributions (dashed-dot-dashed bold lines) were calculated by subtracting the spectra that represent the Trp contribution from those obtained upon excitation at 275 nm. Fluorescence emission units are arbitrary.

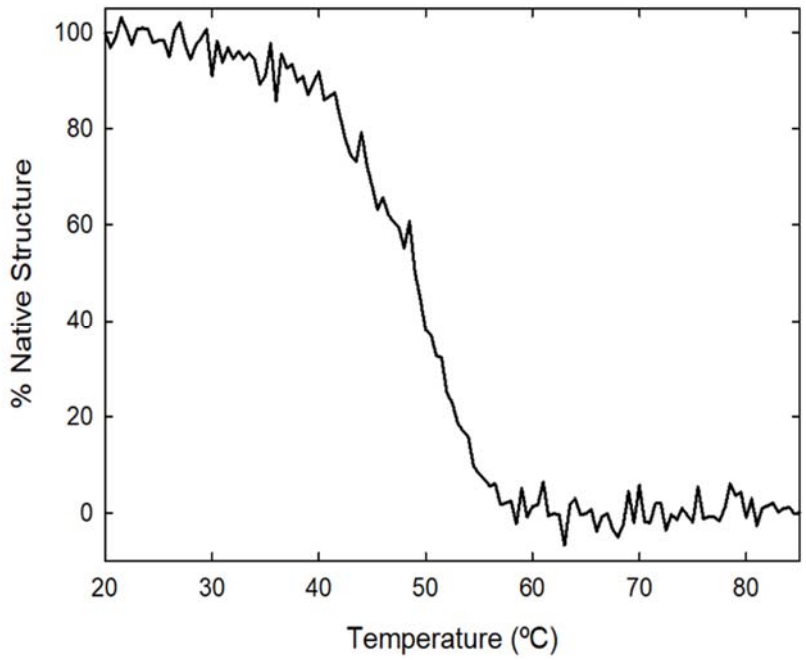

Figure 7. Thermal denaturation profile of StnIII. Measurements were performed by continuously recording the mean residue weight ellipticity at 220 nm (θ_{MRW}). These ellipticity values were used to calculate the percentage of native protein at each temperature.

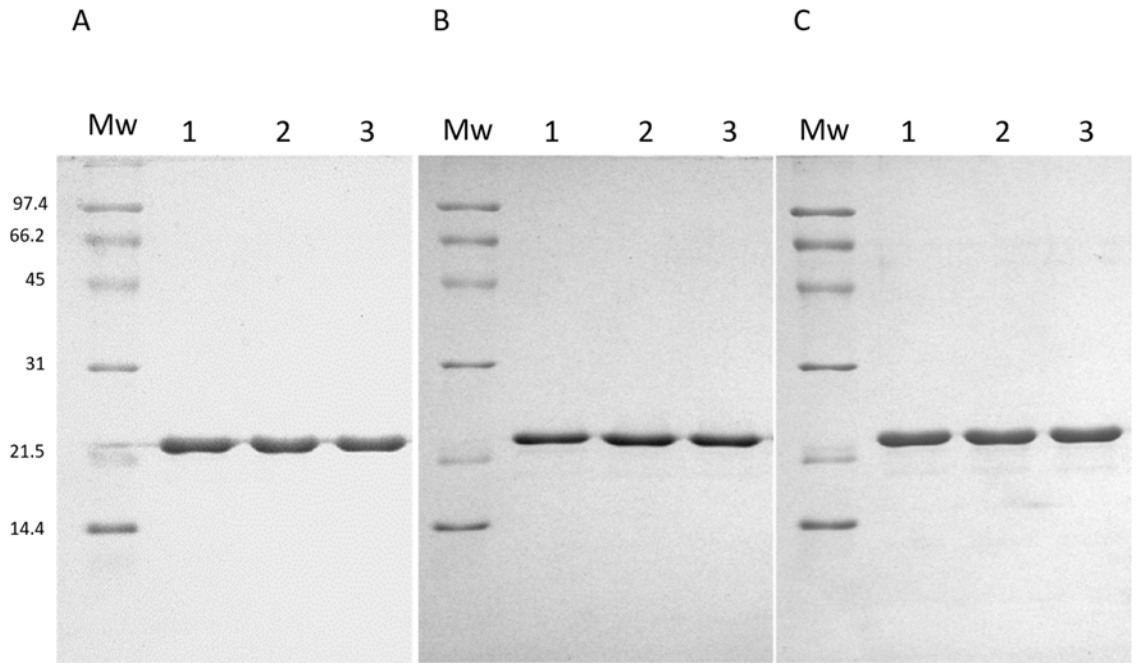

Figure 8. Stability study of StnIII. SDS-PAGE analysis of actinoporin solution preparations maintained at 4 ˚C(1), -20 ˚C (2), and -80 ˚C (3) for 24 h (A), 72 h (B), or 1 week (C). (Mw) Molecular weight standard (Low-Range SDS-PAGE Standards - Biorad) were also loaded, and the corresponding molecular masses are indicated in kDa at the left margin

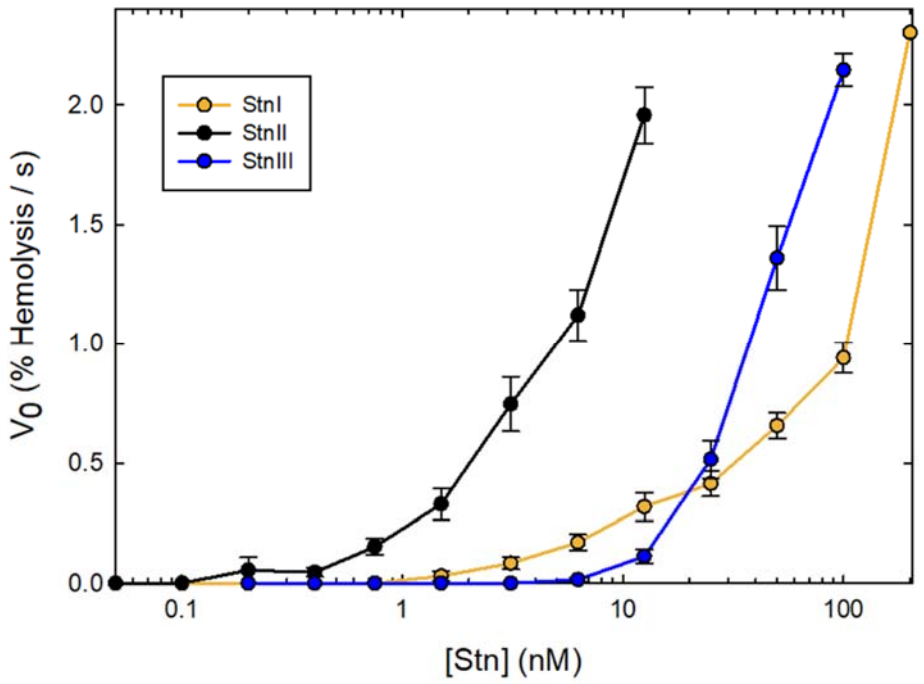

Figure 9. Hemolytic activity of StnI (orange), StnII (black) and StnIII (blue) expressed as the maximum initial hemolytic rate (% hemolysis/s) as a function of different Stn concentrations ranging from 0.1 nM to 100 nM. Values are average of n = 3 ± SEM.

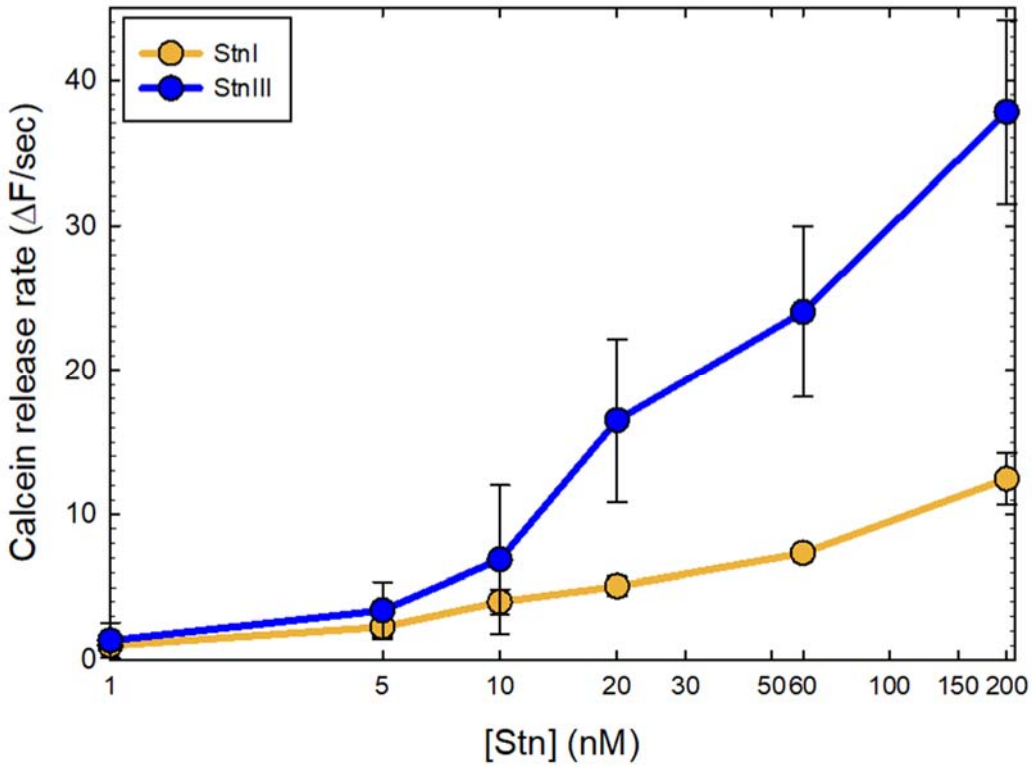

Figure 10. Maximum initial rates of calcein release from DOPS:SM:Chol (1:1:1) vesicles, showed as normalized fluorescence intensity increment/s, as a function of different concentrations of StnI (orange) and StnIII (blue). Values are average of n = 3 ± SEM. Data for StnII are not shown to ensure proper visualization of StnI and StnIII differences, given that StnII is much more active.

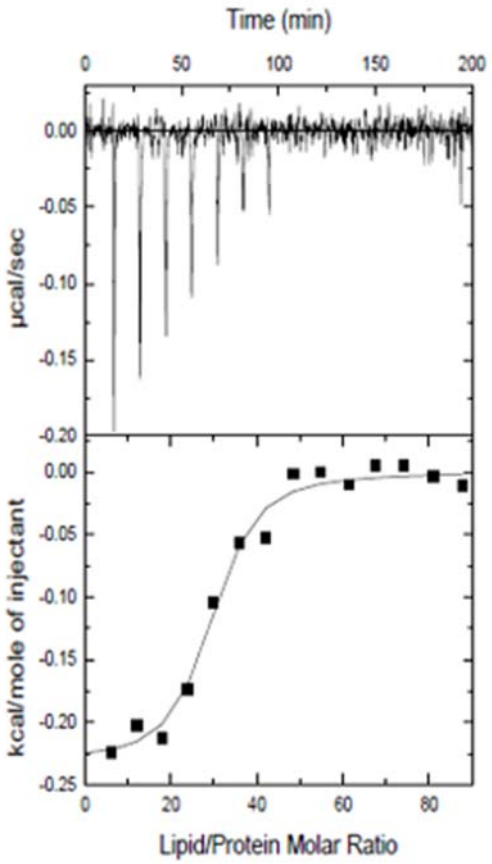

Figure 11. Binding of StnIII to DOPC:SM:Chol (1:1:1) vesicles studied by ITC. Reactant concentrations were 5 µM of StnIII and 3 mM of lipids. Binding isotherms were adjusted to a model in which protein membrane binding involves the participation of "n" lipid molecules as described [31]. The c values ($c = K_a \times P_0$) for the graphs shown is within the range 1–1000.